To Appear in ApJ

RAPID CHANGE OF δ SPOT STRUCTURE ASSOCIATED WITH SEVEN MAJOR FLARES

CHANG LIU[1], NA DENG[1], YU LIU[2], DAVID FALCONER[3], PHILIP R. GOODE[1], CARSTEN DENKER[1], and HAIMIN WANG[1]

Version 3 -- November 23, 2004 -- CL45@NJIT.EDU

ABSTRACT

A large fraction of major flares occur in active regions that exhibit a δ configuration. The formation and disintegration of δ configurations is very important in understanding the evolution of photospheric magnetic fields. In this paper, we study the relationship between the change in δ spot structures and associated major flares. We present a new observational result that part of penumbral segments in the outer δ spot structure decay rapidly after major flares; meanwhile, the neighboring umbral cores and/or inner penumbral regions become darker. Using white-light (WL) observations from the *Transition Region and Coronal Explorer* (*TRACE*), we study the short-term evolution of δ spots associated with seven major flares, including six X-class flares and one M-class flare. The rapid changes, which can be identified in the time profiles of WL mean intensity are permanent, not transient, thus are not due to flare emission. The co-aligned magnetic field observations obtained with the Michelson Doppler Imager (MDI) show substantial changes in the longitudinal magnetic field associated with the decaying penumbrae and darkened central areas. For two events, where vector magnetograms were available, we find that the transverse field associated with the penumbral decay areas decreased while it increased in the central darkened regions. Both events also show an increase in the magnetic shear after the flares. For all the events, we find that the locations of penumbral decay are related to flare emission and are connected by prominent *TRACE* post-flare loops. To

[1]Center for Solar-Terrestrial Research, New Jersey Institute of Technology, University Heights, Newark, NJ 07102-1982

[2]Kwasan and Hida Observatories, Kyoto University, Yamashina-ku, Kyoto 607-8471, Japan

[3]Marshall Space Flight Center, SD50, Huntsville, AL 35812

explain these observations, we propose a reconnection picture in which the two components of a δ spot become strongly connected after the flare. The penumbral fields change from a highly inclined to a more vertical configuration which leads to penumbral decay. The umbral core and inner penumbral region become darker as a result of increasing longitudinal and transverse magnetic field components.

Subject headings: Sun: activity — Sun: flares — Sun: corona — Sun: magnetic fields — sunspots

1. INTRODUCTION

The scientific term δ sunspot was introduced by Künzel (1960) and is defined as umbrae of opposite polarity lying in a common penumbra. δ spots have been known as the most active spot configuration. For over three decades, the morphological evolution of δ configurations and their strong connection to intensive flare activity have been widely studied by many authors (Zirin & Tanaka 1973; Tang 1983; Hagyard et al. 1984; Zirin & Liggett 1987; Zirin 1988; Tanaka 1991; Wang 1992; Tang & Wang 1993; Zirin & Wang 1993; Gaizauskas et al. 1994, 1998; Martínez Pillet et al. 1994; Schmieder et al. 1994; Shi & Wang 1994; Li et al. 1999; Sammis et al. 2000; Liu & Zhang 2001, 2002; Kurokawa et al. 2002). Using eighteen years of observations at Big Bear Solar Observatory (BBSO), Zirin & Liggett (1987) summarized the development of δ spots and classified them in three categories, concluding that δ groups are responsible for almost all great flares. Schmieder et al. (1994) made precise measurements of spot motions in active region AR 6659 during June 1991 to understand the fragmentation of the main δ spot group with time. They found that this fragmentation leads to a continuous restructuring of the magnetic field pattern while rapid changes are evidenced due to fast new flux emergence. The first process leads to sheared field lines and the second process triggers the release of the stored free magnetic energy.

At the same time, solar physicists have been studying flare-related changes in photospheric magnetic fields for nearly four decades (Severny 1964; Zvereva & Severny 1970; Moore et al. 1984; Kosovichev & Zharkova 1999, 2001; Wang & Tang 1993; Wang et al. 1994), which would provide crucial information as to how an active region stores and releases its energy. However, the role of photospheric magnetic fields is still far from being fully understood and is an area of ongoing research. Only recently have rapid and permanent changes of photospheric magnetic fields been observed to be associated with large solar flares (Kosovichev & Zharkova 2001; Spirock et al. 2002; Wang et al. 2002a,b, 2004b; Yurchyshyn et al. 2004). These studies show that high cadence ($\sim$1 minute) and high spatial resolution ($\sim 1''$–$2''$) magnetic field observations reveal sudden flux changes associated with X-class and M-class

flares.

Other than doing the polarization measurements of magnetograms, Deng et al. (2003) first tried a more straightforward approach focusing on changes of the WL structure in flaring active regions. Since most great flares are associated with a δ configuration, they noticed that an entire δ spot region was undergoing rapid change when they studied the X2.3 flare in active region AR 9026 on 2000 June 6. In particular, two penumbral segments decayed rapidly right after the flare. Wang et al. (2004a) studied two more X-class flares, which occurred recently in active region AR 10486 and found very similar penumbral decays. We speculate that this phenomenon may not be restricted to specific active regions, thus, it is only natural to look for similar signatures associated with other flares. We have initiated a statistical study and in this paper, we present the results of our first seven events. Note that our selection of the seven events is not entirely random, because *TRACE* only has a part view of the Sun and its WL observation is not available for every flare activity. Our preliminary result in the recent study also shows that penumbral decay is more likely to be detected when associated with large solar flares (Chen et al. 2005). In addition to the observational results, we propose a reconnection picture for δ spots to interpret our findings. We focus on WL difference images between post-flare and pre-flare states illustrating the penumbral decay and darkening of neighboring umbral cores and inner penumbral region, which will subsequently be related to flare energetics. The evolution of δ spots that we are presenting is an impulsive change, which is closely related to major flares. Therefore, it is quite different when compared to the studies of long-term evolution of δ spots.

We introduce the data used in this study in §2 and subsequently describe the penumbral decay associated with each event in §3. For the X10 flare on 2003 October 29 and X5.3 flare on 2001 August 25, we give a more detailed analysis using vector magnetograms. In §4, we summarize all our findings and propose a Sweet-Parker type (Sweet 1958; Parker 1963) reconnection picture for δ spots based on the observational results.

2. OBSERVATIONS AND DATA PROCESSING

The key data that we are presenting are *TRACE* (Handy et al. 1999) 5000 Å WL images. Other data include *TRACE* Fe IX/X 171 Å and Fe XII/XXIV 195 Å images, full disk magnetograms by MDI (Scherrer et al. 1995) on board the *Solar and Heliospheric Observatory* (*SOHO*, Domingo et al. 1995), vector magnetograms obtained at Marshall Space Flight Center (MSFC) and BBSO, and hard X-ray time profiles and images of the *Reuven Ramaty High Energy Solar Spectroscopic Imager* (*RHESSI*, Lin et al. 2002).

We used standard *TRACE* calibration procedures to process the *TRACE* data. Since *SOHO* has very strict pointing requirements to support its helioseismology experiments, we further aligned *TRACE* WL images with respect to *SOHO*/MDI intensitygrams. We then identified the penumbral decay associated with each event by carefully examining the morphological evolution of the flare active region. First, one WL image near the peak time of the flare was chosen, and WL images from well before to well after the flare were differentially rotated to that time using standard procedures in *SolarSoft* (*SSW*, Freeland & Handy 1998). Then, we made movies using the co-aligned WL images and were able to unambiguously trace the evolution of major spots. Meanwhile, *SOHO*/MDI offers high temporal resolution (1 min) full-disk magnetogram data with $\sim 4''$ spatial resolution. Combined with the corresponding *TRACE* WL images with $1''$ spatial resolution and typical temporal resolution of 1.5-2.5 minutes, we can easily identify the magnetic polarity and position of a spot, and calculate the time profiles of intensity and magnetic flux of a specific region. *TRACE* also provides unprecedented observations of the outer solar atmosphere. Thus enabling us to observe a corona that is extremely dynamic and full of flows and wave phenomena. The rapidly evolving loops generally outline the coronal magnetic field. Therefore, we tried to use coronal images in *TRACE* 171 Å and 195 Å to study any change in the coronal environment between post-flare and pre-flare states. We understand that direct evidence for magnetic reconnection in flares may be difficult to find, despite the fact that it is thought to be the primary process behind flares. But since the reconnection appears to be (largely) completed by the time the post-flare loop system are detected by *TRACE* (Schrijver et al. 1999), we carefully searched for any obvious changes, especially for newly formed loops. We then can deduce a complete picture of the flare combined with our observational results in photosphere and chromosphere.

For the 2003 October 29 event, we used MSFC vector magnetograph data. The magnetograph is a filter-based instrument employing a tunable Zeiss birefringent filter with a 0.125 Å bandpass and an electro-optical modulator to obtain integrated Stokes profiles in the Fe I 5250 Å absorption line. The field-of-view (FOV) of the instrument is $7' \times 5'$ and the spatial resolution is $1.28''$ per pixel. For the 2001 August 25 event, we used data from BBSO's digital magnetograph (DVMG) system, which typically covers an area of about $5'$ $\times$ $5'$ with $\sim 0.6''$ pixel resolution. The BBSO data reduction procedure is discussed in detail by Wang et al. (2002b).

To show the temporal evolution of the flares and understand the relationship between the rapid changes of magnetic fields and energy release sites, we use hard X-ray time profiles and images from *RHESSI* for the three events that occurred in 2003. Among the other four events, two have complete hard X-ray coverage by the *Yohkoh* Hard X-ray Telescope (HXT) and have been studied in detail by other authors.

3. RESULTS

For each event, we started with an analysis of the difference image (post-flare minus pre-flare state) in *TRACE* WL, which was smoothed by a window of $10'' \times 10''$ in order to magnify the morphological changes by smoothing out the background pattern caused by granulation and five minute oscillation. Any bright feature in the difference image indicates a brightening in the post-flare image, e.g., an area of decayed penumbra that fades into the granular background, whereas any dark feature corresponds to a darkening in the post-flare image, e.g., the darkening of either an umbral core or an inner penumbral area. With the aid of difference images, we can identify and trace the decaying and darkening regions in the time-lapse WL movies. Please note that the difference image sometimes may be affected by proper motions of features. Therefore, we ultimately rely on the time-lapse movies to pin down the exact location of the decaying (labeled "D" in figures) and darkening regions (labeled "E" in figures). Then we made time profiles of mean intensity for both the decaying and darkening areas. The mean intensity is defined as the average intensity of a certain area outlined by a box normalized to the photospheric intensity outside the sunspot in a quiet Sun region. We also studied the evolution of the line-of-sight magnetic fields associated with these regions by first creating movies using the corresponding MDI 1-minute cadence data and subsequently integrating the magnetic flux within each box. To link the temporal evolution of the flare, we further superimposed the hard X-ray time profile or the derivative of the soft X-ray lightcurve onto the time profiles of the magnetic flux change.

Table 1 lists the seven flare events that were analyzed. For each of them, we located two penumbral decay regions and one central darkening region. Note that Deng et al. (2003) and Wang et al. (2004a) have discussed event No. 1 and events No. 1, 5, and 6, respectively. Here we extend these studies and include other events to assemble a unified picture of penumbral decay. In addition to some general information about each event, we provide in Table 1, the mean intensity changes $\Delta I_{D1,2}$ for the decaying areas D1 and D2 and ΔI_E for the central darkening region E, the amount of magnetic flux change $\Delta F_{D1,2}$ in the penumbral decay areas D1 and D2, and the magnetic flux changes $\Delta F_{E+,-}$ for positive and negative polarities of the central darkening region E. We only present time profiles of mean intensity and magnetic flux for the 2003 October 29 event (Figure 2) and summarize the results of the other events in Table 1. First, we will present the three events which occurred in active region AR 10486 before discussing the remaining four events. Note that in all figures, we corrected image shift due to solar rotation. *TRACE* 1600 Å and EUV intensities are presented as negatives in order to optimize the visibility of flare structure.

3.1. Detailed Study of the 2003 October 29 X10 Event

This X10 event was well-covered by many space and ground-based instruments. Along with other great flares in the active region AR 10486, it is being extensively scrutinized by the solar physics and space science community. Wang et al. (2004a) first reported the decayed penumbra associated with this event and the X17 event of 2003 October 28. After careful data alignment, we find another penumbral decay area for each of the events. Figure 1 compares the morphology between post-flare and pre-flare states in both *TRACE* WL and 195 Å for this X10 event. From the WL difference image shown in Figure 1(c), we identify two penumbral decay areas D1 and D2 and the darkening central region E. Figure 1(d) shows the WL image at flare maximum with superimposed *RHESSI* hard X-ray contours in the 50-100 keV channel obtained during the peak of the flare. It can be clearly seen that the two penumbral decay regions are co-spatial with two flare kernels in WL and hard X-rays. We noticed that the much stronger eastern flare kernel is near the very prominent penumbral decay area D1, while the weaker western kernel is near the less prominent area D2. Note that the positions of hard X-ray footpoints in Figure 1 are a snapshot at the flare peak time. The footpoint motions during the flare was studied in detail by Krucker et al. (2005). The two frames of *TRACE* 195 Å images, although with different exposure times, show that after the flare, strong post-flare loops newly formed within the δ spot region, which is outlined by the large box in Figure 1(e, f). In Figure 2, we analyzed the intensity and magnetic evolution of these areas. The error bars in the top panel are standard deviation determined for *TRACE* WL images by calculating the fluctuation in the time profile of mean intensity in a quiet Sun region. An intensity of 1.0 represents the quiet Sun intensity. Thus, a large value represents a smaller and/or lighter sunspot in the area. For the areas D1 and D2, it is obvious that their mean intensity increases very rapidly (6.3% and 4.6%, within $\sim$30 minutes) after the flare, representing the rapid penumbral decay in these two regions. We monitor this change even longer after the flare ($\sim$10 hrs) and find that the decaying penumbrae remain un-restored. With similar results for other events that will be discussed later, this means that the penumbral decay is not only rapid, but permanent, compared to the time scale of the flare itself. Moreover, the mean intensity for the central region E1 decreased rapidly and permanently by 3.1% after the flare, indicating the feature is becoming darker. After a close inspection of the time-lapse movie, we find that these darkening features actually include two kinds: one is the neighboring umbral core, another is the inner penumbra. However, in some events, only the inner penumbral region becomes darker after the flare. Figure 2 also shows substantial changes of longitudinal magnetic fields associated with the decaying and darkening areas. These changes are well related to the flare.

In Figure 3, we compare the MSFC vector magnetograms before and after the flare. The decrease in transverse field strength associated with the cusp-like penumbral decay area

D1 and the increase in the central region across the magnetic neutral line is obvious. In Figure 4, we further align the MSFC data with the *TRACE* pointing presented in Figure 1. We find that the mean transverse field strength within areas D1 and D2 decreased by 173 G and 56 G, respectively, and increased by 97 G in area E. For the small region across the magnetic neutral line (indicated by two white brackets in the panels e and f), the weighted mean magnetic shear angle increased by 10° after the flare (see also Figure 3 lower panels). This shear angle is defined as the angular difference between the potential and the measured transverse fields, weighted by the measured transverse field strength. The mean inclination angle has no substantial change within area D2, but increases by 12° within area D1. As we will discuss later, the study of vector magnetograms of 2001 August 25 event reveals similar results.

3.2. Other Events

3.2.1. 2003 November 2 X8.3 Event

This flare occurred when active region AR 10486 approached the west limb (S14, W56). Although the morphology of the whole region has changed dramatically, the flare is still related to the δ configuration in the eastern part of the whole sunspot group, which is identical to the location of the X10 flare on 2003 October 29. The difference image in Figure 5 shows two penumbral decay areas D1 and D2 and the central darkening region E, which is predominantly in the form of penumbra. *TRACE* WL images have a data gap between 17:11 UT and 17:39 UT, thus missed the flare peak around 17:25 UT. By examining the time-lapse movie, we find that right before the data gap, there were discernible WL flare kernels, which begin to glow. In Figure 5(d), a little black box is drawn around a WL flare kernel which is found to move across the penumbral decay area D1. The superimposed *RHESSI* hard X-ray contours are also associated with the penumbral decay areas. Similar to the 2003 October 29 event, the stronger northern hard X-ray kernel is associated with the stronger penumbral decay area D1. The images in *TRACE* 195 Å show the evolution of the coronal loops, which we can observe more clearly for this near-limb event. We find that early in the event (Figure 5e), loops were linking the northern spot to the area outside of the entire active region. After the reconnection (Figure 5f), new loops formed within the δ spot region connecting the northern and southern spots.

3.2.2. 2003 October 28 X17 Event

Although the cadence of *TRACE* WL images is low (∼1 hr) for this flare, we are still able to find the decaying penumbra by comparing two WL images, one before the flare (Figure 6a) and another well after the peak (Figure 6b). The difference image (Figure 6c) shows a strong penumbral decay area D1, while the decaying area D2 is not that obvious. The darkening region E includes both the umbral core and inner penumbral regions. Since the WL image at flare maximum is not available, we present a *TRACE* 1600 Å image instead in Figure 6(d) and superimpose *RHESSI* hard X-ray contours in the 50-100 keV range. Obviously, penumbral decay area D1 is related to a section of one of the two *TRACE* 1600 Å flare ribbons, while the less obvious penumbral decay area D2 is near one of the two hard X-ray sources but does not coincide with it. *TRACE* 195 Å images show a dramatic evolution of post-flare loops (Figure 6f) over the δ configuration region that is related to the flare.

3.2.3. Re-Evaluation of the 2000 June 6 X2.3 Event

Deng et al. (2003) discussed this event in detail and found two penumbral areas that very obviously decayed right after the flare. Since this event is associated with filament eruption, they tried to interpret the penumbral decay phenomenon in the context of the magnetic breakout model (Antiochos et al. 1999) for CMEs and eruptive flares. The difference image clearly showing the decaying and darkening regions was later presented by Wang et al. (2004a). By carefully examining the evolution in *TRACE* EUV images, we find that the morphology of the coronal loops is substantially different between post-flare and pre-flare states, and reconnection shown as orientation changes of coronal loops is very similar to the other six events in this study. Thus, this event also fits into our unified picture that is different from the breakout scenario and will be discussed in the next section. Figure 7(a) shows the pre-flare state of the complicated active region AR 9026, which has a δ configuration. Two northern spots have positive magnetic polarity, two southern spots negative. Figure 7(f) shows post-flare loops that clearly connect the two sunspot regions on both sides of the neutral line and this connection extends to the penumbral decay regions D1 and D2, which are quite different from pre-flare state shown in Figure 7(e). The WL image near flare maximum is presented in Figure 7(d), in which two WL flare kernels (as indicated by two arrows) are discernible. These two WL kernels are later found to separate, sweeping through the two penumbral decay areas D1 and D2. Unfortunately, there were no hard X-ray images available for this event.

Recent work reveals very similar penumbral decays associated with an X1.2 flare on

2000 June 7 in this active region (Chen et al. 2005). In contrast to these impulsive changes, Kurokawa et al. (2002) constructed a realistic model of a strongly twisted flux rope to explain the drastic evolution of this flare-productive active region in about five days. In particular, they reported the catastrophic decay of the central δ spot region from 10:00 UT of June 6 to 16:00 UT of June 7. Thus it is very meaningful to combine impulsive change and long-term evolution of δ configurations in the next study (e.g., Wang et al. 2005).

3.2.4. 2001 April 6 X5.6 and April 9 M7.9 Events

These two flares occurred in the same active region (AR 9415) and were associated with the same δ spot. *TRACE* WL observations covered both flares, with a short temporal data gap during the flare maximum. The difference images for both events (Figure 8c and 9c) show a similar ring-like structure: bright in the outer edge of the δ spot, indicating penumbral decay and dark in the center, indicating the darkening umbral core and inner penumbra. Furthermore, the evolution in *TRACE* 171 Å images for both events clearly shows that after the flare, strong loops exist within the δ configuration so that the two spots constituting the δ spot become strongly connected. Compared with the post-flare state, this kind of connection is hardly seen in the pre-flare images. By studying *Yohkoh* Soft X-ray Telescope (SXT) images, Yurchyshyn (2003) also reported this obvious connectivity change for the 2001 April 9 event. As shown in Figure 8(d) and 9(d), flare ribbons in *TRACE* 1600 Å were associated with the penumbral decay areas for both events. *Yohkoh* HXT observations were available for the April 6 event and were presented by Qiu et al. (2004). They recognized three flare kernels in the HXT H channel (53-93 keV) and all three kernels were found inside the sunspot umbrae in the active region. The strongest of these flare kernels is located near the central darkening area E in our result.

3.2.5. 2001 August 25 X5.3 Event

This WL flare was discussed in detail by Metcalf et al. (2003), in which they found three flare kernels in the HXT M2 channel (33-53 keV). Two of the flare kernels are near the penumbral decay area D1 shown in Figure 10. Using BBSO data, Wang et al. (2002b) studied photospheric magnetic field changes associated with this flare and concentrated on the central region along the neutral line that is near the darkening area E in our study. As they pointed out, the central darkening region is predominantly in the form of penumbra. Besides this, the difference image in our study clearly shows two penumbral decay areas D1 and D2 in the outer δ spot structure. We re-examined the BBSO vector magnetogram data

and find that the mean transverse field strength within the penumbral decay areas D1 and D2 decreased by 21±10 G and 36±6 G, respectively, and increased by 113±21 G in the central darkening area E. Although the changes of transverse field associated with the areas D1 and D2 are on the order of the sensitivity of the BBSO DVMG system, we find that it is nonetheless statistically meaningful by plotting their time profiles. Moreover, the weighted mean magnetic shear angle within area E rapidly increased by 10° after the flare. Note that in Figure 10(a), the magnetic abnormality near area D1 (and some other locations as well) is due to very inclined magnetic field lines and effect of projection. The time profile of MDI magnetograms shows that after the flare, the negative polarity within the area D1 increased while the positive decreased. Taking into account the decreasing transverse field, we deduce that the mean inclination angle within the area D1 becomes larger, i.e., the magnetic field turns more vertical. However, we do not find a significant change of the inclination angle within the area D2. Figure 10(d) shows the *TRACE* WL image near flare maximum. We find that the two WL flare ribbons separate and sweep through the two penumbral decay regions. Again, the evolution in *TRACE* 171 Å images shows similar magnetic structures that connected the two spots after the flare.

4. SUMMARY AND DISCUSSION

We have presented observations of rapid structural changes within seven δ spots, each associated with a major flare, by monitoring the evolution in *TRACE* WL. Our major findings are:

1. The time-lapse movies show that for each event, the δ spot appears to have "shrunk" after the major flare. Accordingly, we find that part of the penumbral segments in the outer δ structure decayed and the neighboring umbral core and/or inner penumbral region near the magnetic neutral line darkened. We did not find such short-term changes to the δ spot when there was no major flare.

In contrast to previous studies of long-term evolution covering time periods of hours to days, the changes of the δ spot structure presented in this study are rapid and well associated with major flares. The difference images for all the seven events show a very similar pattern with a bright (decaying) region outside and a darkening in the center. Thus, we argue that the changes observed by us and others are real.

2. The increasing mean intensity in the penumbral decay areas and decreasing intensity of darkening regions are ∼2-7% above the quiet Sun photospheric intensity. These changes are coincident with the impulsive hard X-ray emissions of the related major flares. More

importantly, these changes are permanent, not transient. Figure 11 shows the scatter plot of the average intensity change of penumbral decay against *GOES* X-ray flux, from which we can clearly see the trend that the larger the flare size, the stronger the penumbral decay is. We will further investigate this point with more statistical significance (Chen et al. 2005).

The decayed and darkened features are best seen in the time-lapse *TRACE* WL movies. The calculation of the mean intensity of these regions also show a clear increase or decrease, which coincide with the peak in the hard X-ray emission. A natural explanation of penumbral decay is that it could be associated with heating of the lower atmosphere due to the flare. However, we argue against such an explanation mainly because that the decayed penumbra is not restored even several hours after each event (Wang et al. 2004a).

3. The locations of the penumbral decay are associated with flare emissions, albeit with distinct differences for each event. WL flare kernels or ribbons are coincident with or sweep through the penumbral decay regions in the events 1, 4, 6, and 7. WL observations at flare maximum were not available for the events 2 and 3, however, the decay regions in these two events are all near *TRACE* 1600 Å flare ribbons. *RHESSI* hard X-ray sources are associated with both penumbral decay regions in events 6 and 7. One of the decay regions in event 5 is near the hard X-ray source, while another is related to one of the two *TRACE* 1600 Å flare ribbons.

4. The post-flare loops observed in *TRACE* EUV wavelengths "predominate" the δ spot, suggesting that the two components of the δ spot become strongly connected after reconnection.

The nature of post-flare loops in dynamic flares has been an interesting subject for quite a long time. The classical CSHKP model (Carmichael 1964; Sturrock 1966; Hirayama 1974; Kopp & Pneuman 1976) interprets the post-flare loop systems as a result of the reconnection of magnetic field lines torn open by the flare event. According to this model, the magnetic configuration of the corona overlying the flare site contains many closed loops prior to the flare and this original configuration is restored through the reconnection after the flare. However, this can hardly explain the changes of photospheric features observed by us. In our picture that will be presented next, the magnetic field geometry is altered drastically after the flare, which we believe leads to the penumbral decay and central region darkening.

5. Vector magnetogram analysis of the 2003 October 29 and 2001 August 25 events both show that the transverse magnetic field decreases in the penumbral decay area while it increases in the central darkening region, which directly support our observational results of decayed and darkened penumbrae. Remarkably, the magnetic shear in both events shows an increase by 10° after the flares.

6. The longitudinal magnetic fields associated with the decaying and darkening regions also exhibit substantial changes after the flares.

We further elaborate the interpretation proposed by Wang et al. (2004a) that the penumbral decay is due to changes in magnetic topology in the following way: the magnetic fields become more vertical after the flare and the umbrae become darker as a result of an enhancement of the longitudinal magnetic field. For the six events in our study, we use high-resolution, high-cadence line-of-sight magnetograms from MDI and for the 2001 August 25 event, we use BBSO magnetograms. For each event, we located two penumbral decay regions, which are in opposing magnetic fields and one central darkened region near the magnetic neutral line. We further calculated the changes of magnetic flux associated with the decaying and darkening regions. From the results listed in Table 1, we can see that seven penumbral decay regions have a decreased longitudinal magnetic flux after the flare. We believe this is because that the penumbral field turned more vertical and merged with the umbral field. For the other five penumbral decay regions with increasing longitudinal magnetic flux, we speculate that the penumbral field turned more vertical but did not become sufficiently vertical to darken and become part of the umbral field. For the central darkening regions, the change of longitudinal magnetic flux is not conclusive. Since the central darkening regions usually include the sunspot umbra, we recognize the limitation of filter-based magnetograph systems, which are not well suited for measurements of strong magnetic fields because of Zeeman saturation. Therefore, our conclusions are mainly based on WL observations.

Based on the analysis of the seven events in our study, we therefore put forward a unified reconnection picture for the δ configuration and present a simplified cartoon for this picture in Figure 12. The grey and black lines stand for penumbral and umbral fields, respectively. Thus, we make the following three major points:

I. In the pre-flare configuration, a δ sunspot is the joint of two separate magnetic flux systems. Strong electric current may exist there due to the high field strength and large magnetic gradient.

II. The two spots become strongly connected after the flare, leading the penumbral fields to change from highly inclined in the pre-flare state to a more vertical configuration after the flare. This accounts for the penumbral decay.

III. The umbra becomes darker as a result of an enhanced longitudinal magnetic field. The strong connection between the two spots also leads to a substantial increase in the transverse field in the central δ spot region, which can explain the darkening of the inner penumbra. In events 4 and 6, where vector magnetogram data were available, we do find such an enhancement of transverse fields after the flares.

Note that (1) the pre-flare state in our picture is a simplified condition, because the two components of a δ spot may already have extra connection in the coronal that can support filament. But in either case, the *TRACE* EUV post-flare images of all seven events clearly show that the direct connection between the two spots becomes much stronger after the flare. For the 2000 June 6 event, the associated filament may erupt outward first enabling the field lines of the two spots to connect. (2) Other modifications can be applied to this picture. For example, the strong connection between the two components of the δ spot may result in the emergence of highly twisted flux tubes from beneath the surface, because relaxation of the surface makes flux emergence easier. This can add to the darkening of the central δ spot region and explain the increase of magnetic shear after the flare. Thus our picture, with some appropriate adjustments, could be another explanation of the finding of rapid change of magnetic fields associated with six X-class flares (Wang et al. 2002b). Two events among them have been studied in this paper. (3) Although points II and III are mainly based on two events where vector magnetograms were available, the unified picture can explain all the other events that exhibit similar changes in morphology.

Observations also indicate that penumbral decay tends to recur in some active regions. Events 5, 6, and 7 occurring from 2003 October 28 to November 2 in AR 10486 all exhibit penumbral decay with similar properties. Events 2 and 3 on 2001 April 6 and 9 show another group of penumbral decay occurring at the same δ configuration in AR 9415. Recent work reveals that penumbral decay is also associated with an X1.2 flare on 2000 June 7 in active region AR 9026 (same as event 1 in our study) and the decaying and darkening areas are almost identical (Chen et al. 2005). Furthermore, we have found more active regions that are associated with flare-related penumbral decay while some of them do not have a δ configuration, thus may not fit into our current picture. Extended studies will be made to statistically investigate the relationship between penumbral decay and solar flares (Chen et al. 2005), comparing the observation with photospheric magnetic field extrapolation, and evaluate the consistency of our picture with CMEs.

The authors thank *TRACE*, *SOHO*, *RHESSI*, MSFC, and BBSO teams for providing excellent data sets. We are grateful to the referee for valuable remarks and suggestions that resulted in improvement of the paper. CL also thanks Dr. J. Qiu for reading the entire draft and giving many helpful comments, Dr. V. Yurchyshyn for instructive discussions on interpreting the observations, and Y. Xu for help on preparing the BBSO magnetograms. This work is supported by NASA under grants NAG5-13661 and NNG0-4GG21G and by NSF under grants ATM-0313591 and ATM-0236945.

Table 1. PENUMBRAL DECAY EVENTS

Event No.	Date	Starting (UT)	Peak (UT)	AR	*GOES* Level	Location (deg)	$\Delta I_{D1,2}$ (%)		ΔI_E (%)	$\Delta\lvert F_{D1,2}\rvert$ (10^{19}Mx)		$\Delta\lvert F_{E+,-}\rvert$ (10^{19}Mx)	
1.....	2000 Jun 6	1458	1525	9026	X2.3	N33, E25	4.1	3.7	-5.3	-22±10	∼0[a]	4.5±2	15±7
2.....	2001 Apr 6	1910	1921	9415	X5.6	S20, E31	4.6	3.4	-7.9	10±7	-16±8	∼0[a]	∼0[a]
3.....	2001 Apr 9	1520	1534	9415	M7.9	S21, W04	1.3	3.2	-3.1	∼0[a]	-9.0±4	∼0[a]	17±3
4.....	2001 Aug 25	1623	1645	9591	X5.3	S17, E34	6.6	5.2	-7.5	3.5±1	-17±3	-9.6±2	8.5±2
5.....	2003 Oct 28	0951	1110	10486	X17	S18, E20	6.1	6.2	-5.4	-9.0±7	6.9±2	-11±7	∼0[a]
6.....	2003 Oct 29	2037	2049	10486	X10	S15, W02	6.3	4.6	-3.1	5.5±4	-7.7±2	49±7	-14±7
7.....	2003 Nov 2	1703	1725	10486	X8.3	S14, W56	5.4	5.0	-5.3	-25±3	3.6±0.8	-13±3	13±3

[a]No reliable change is observed, either because the change is small or buried in the long term evolution of magnetic field.

Note. — The results of changes of WL intensity (ΔI) and magnetic flux (ΔF) are obtained by taking the difference between the average values of intensity/flux within 1-2 hours in the pre-flare and post-flare states. The 1 σ statistical error for WL intensity is ∼0.5%, determined by calculating the fluctuation in the time profile of mean intensity in a quiet Sun region. Since MDI data have a noise level of no more than 20 G (Scherrer et al. 1995; Hagenaar 2001), we take (20 G × Area) as a *largest* error to the magnetic flux.

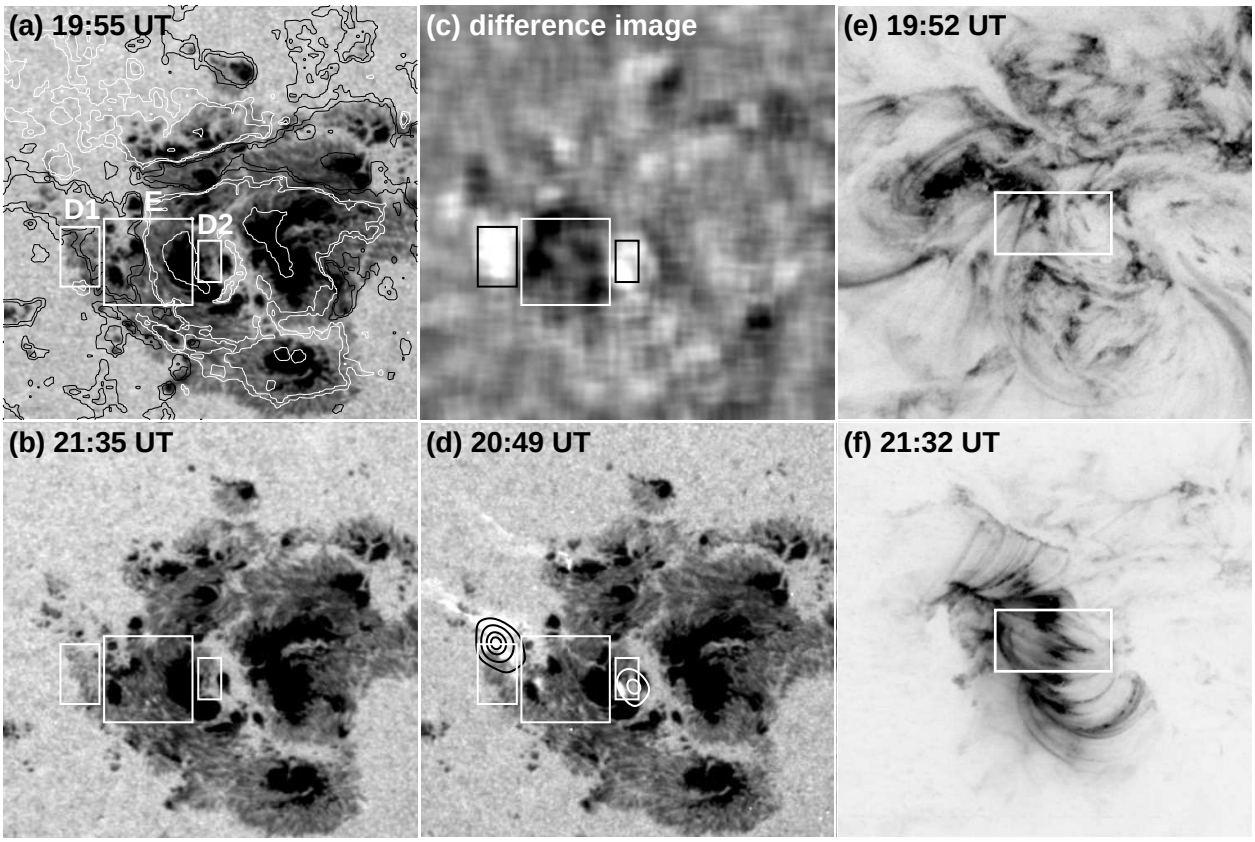

Fig. 1.— Comparison of pre-flare (a, e) and post-flare (b, f) states for the X10 flare on 2003 October 29. (a, b) and (e, f) are *TRACE* WL and 195 Å images, respectively. (c) is the WL difference image (the post-flare image minus the pre-flare image). MDI longitudinal magnetic field is superimposed onto (a), showing the polarity of every spot clearly. The white/black contours represent positive/negative longitudinal magnetic fields, respectively. The magnetic contour levels are ± 150, 300, 1200, and 2400 G. (d) is the WL image at flare maximum with superimposed *RHESSI* 50-100 keV hard X-ray contours (levels are 20%, 40%, 70%, and 90% of the maximum counts) accumulated from 20:49:42 UT to 20:50:42 UT. The FOV of (a-d) is $180'' \times 180''$. (e, f) have a larger FOV ($250'' \times 250''$) to show the complete coronal morphology, in which the large box encompasses the total areas of D1, D2, and E1, outlining the δ spot associated with the flare.

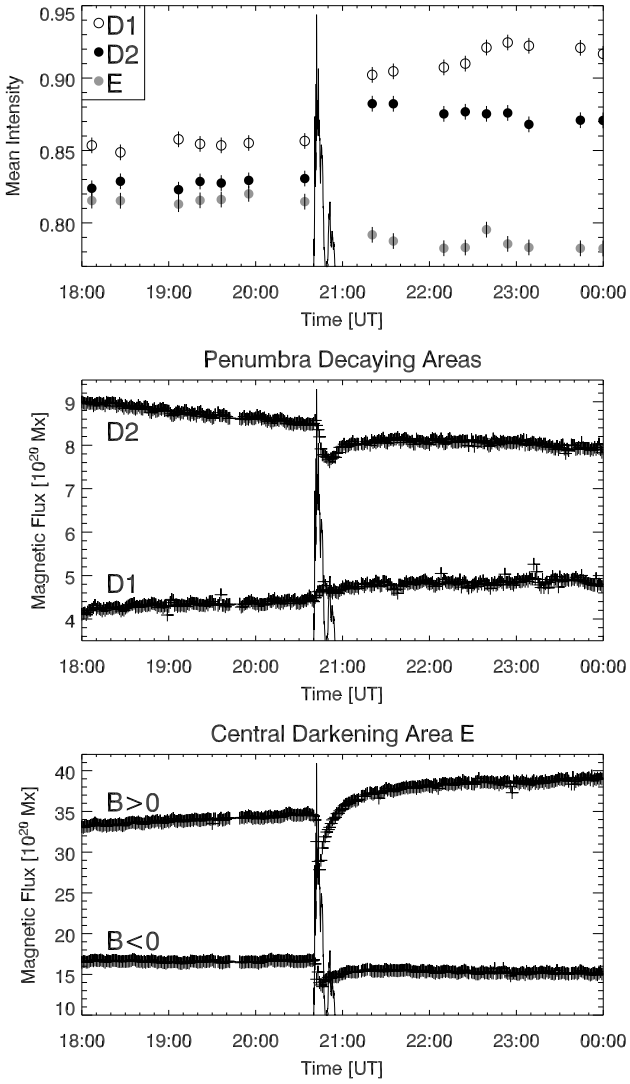

Fig. 2.— *Top panel:* Mean intensity of the penumbral decay areas D1 and D2 and the central darkening area E as a function of time on 2003 October 29. For a clearer representation, the data values of areas D2 and E are added 0.1 and 0.12, respectively. *Middle and bottom panel:* Evolution of absolute value of the longitudinal magnetic flux in each area. The curve of vertical spikes represents the *RHESSI* hard X-ray counts in the 50-100 keV range.

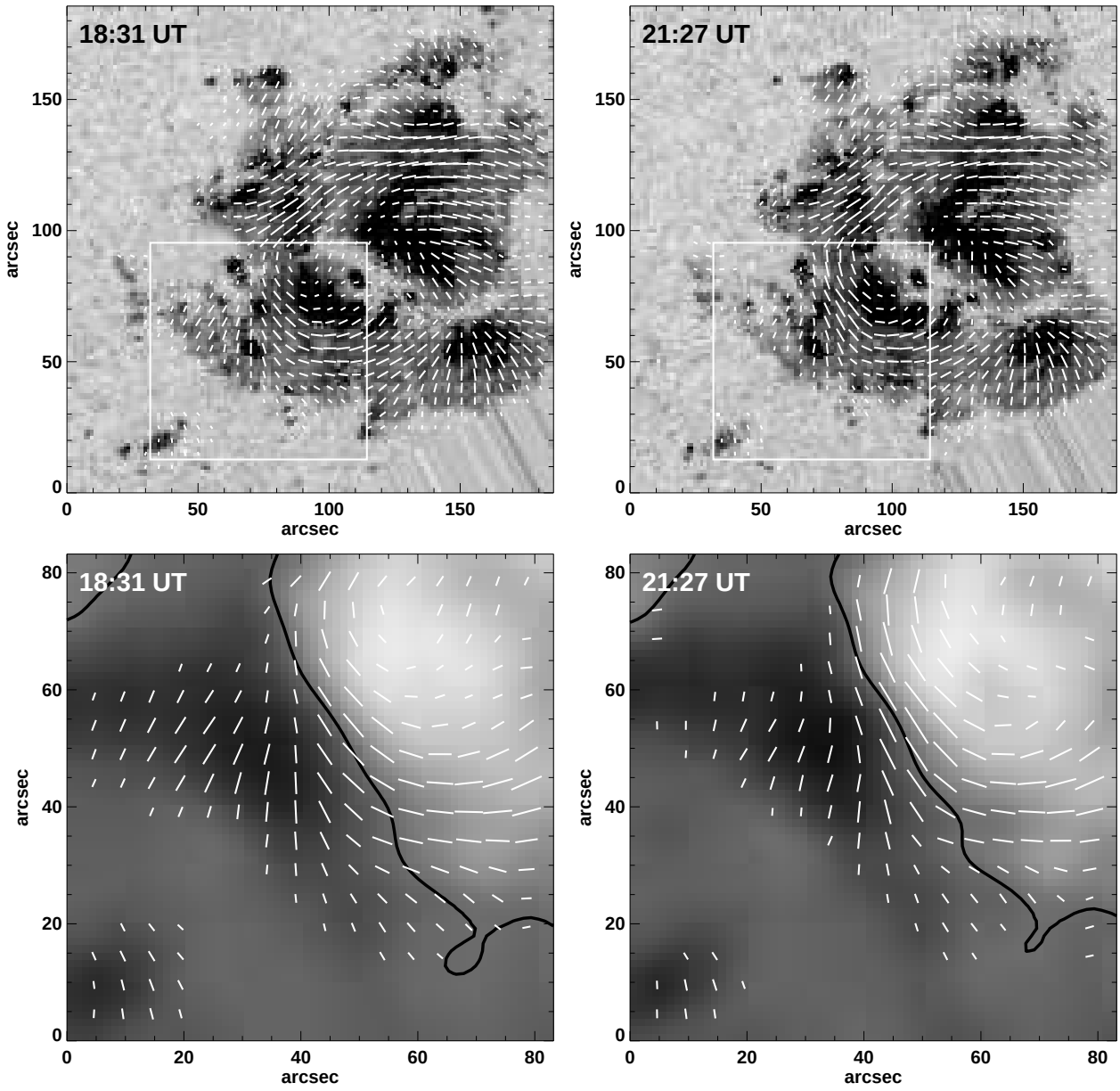

Fig. 3.— *Upper panel:* MSFC vector magnetograms before and after the X10 flare on 2003 October 29 superimposed onto the corresponding *TRACE* WL images at 18:26 UT and 21:35 UT respectively. The white lines are the transverse fields with the length proportional to the field strength. The FOV is $185'' \times 185''$. *Lower panel:* A magnified view of the flare site outlined by the boxes in the upper panel. The black line is the magnetic neutral line where the flare is initiated.

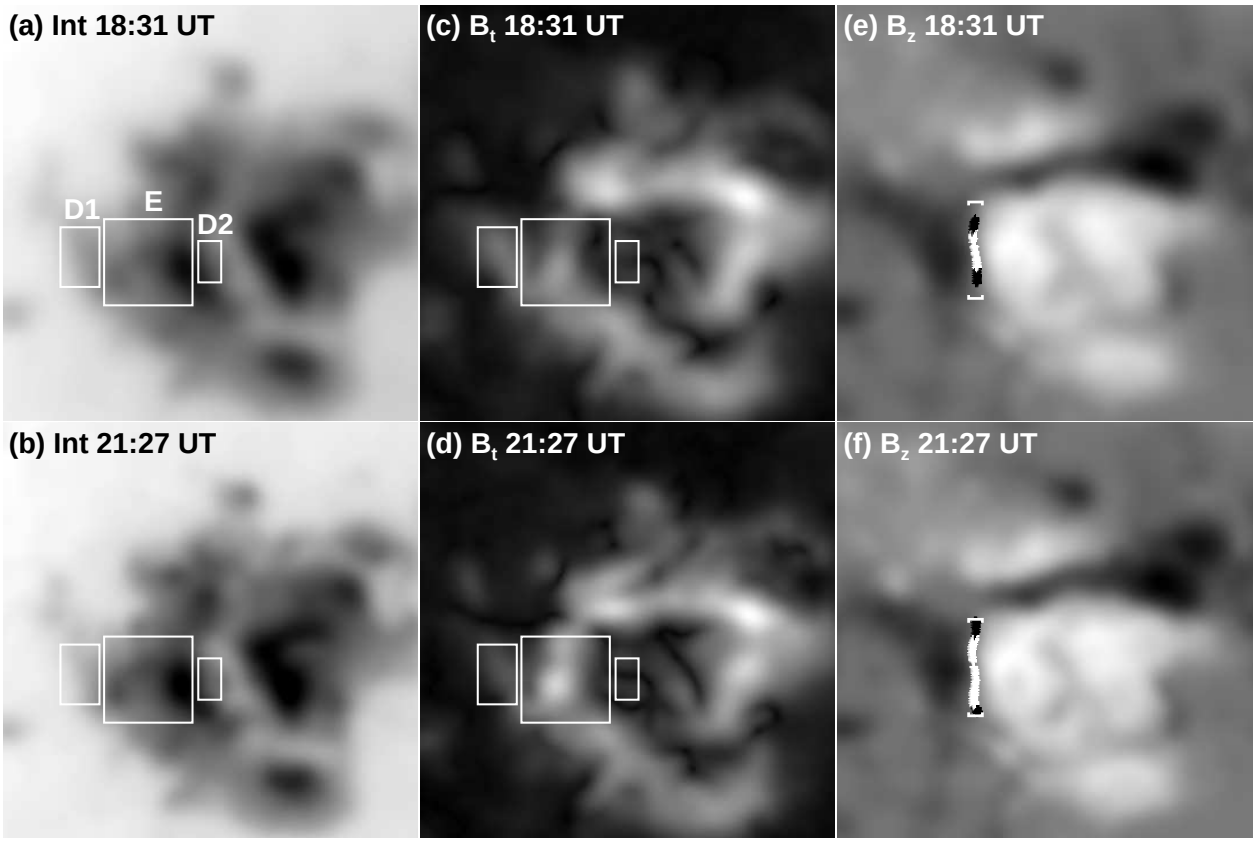

Fig. 4.— MSFC intensity, transverse field, and longitudinal field images before and after the X10 flare on 2003 October 29. The three boxes are the same as in Figure 1. The white brackets in (e) and (f) indicate the length along the neutral line, where the weighted mean magnetic shear angle is calculated. High shear (70-80°) and maximum shear (80-90°) areas are denoted by *black* and *white* plus signs, respectively.

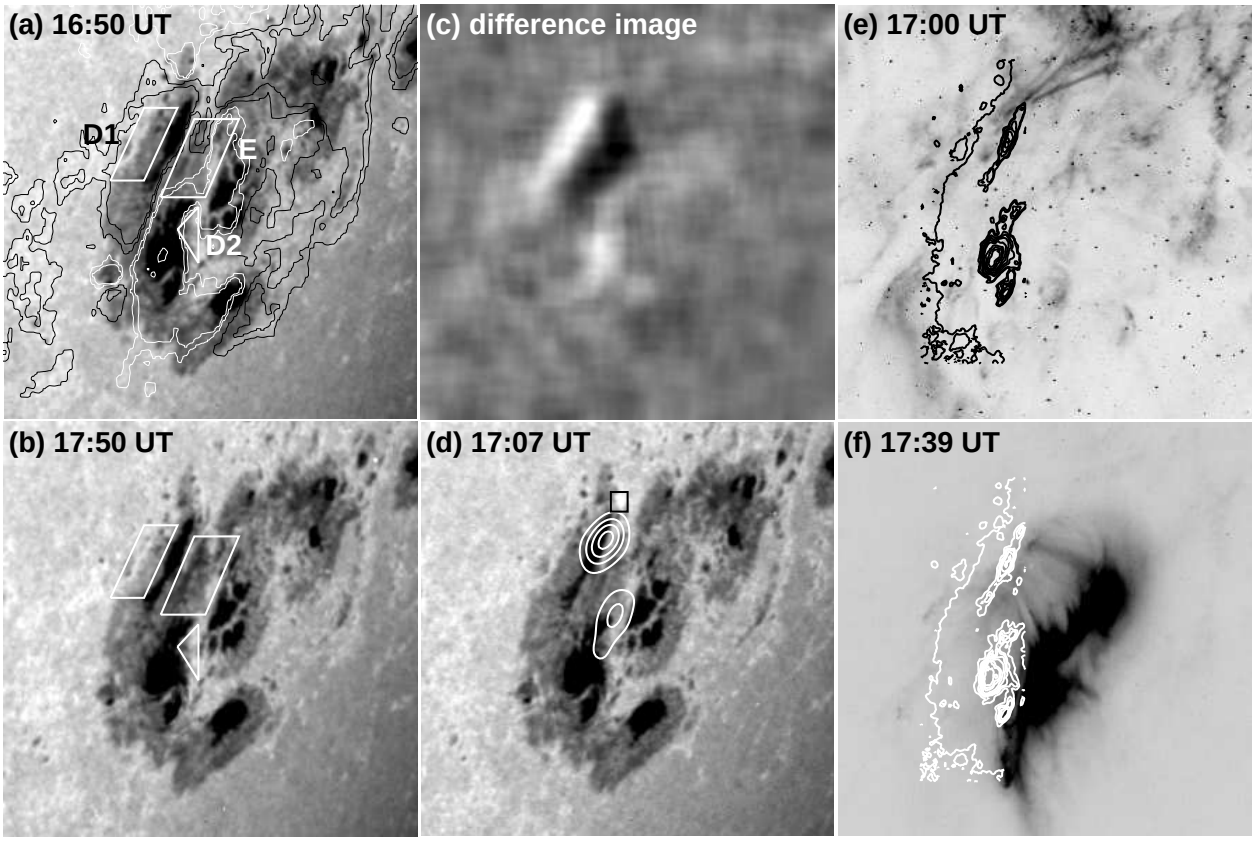

Fig. 5.— Same as Figure 1, but for the X8.3 flare on 2003 November 2. The little black box in (d) indicates the position of a bright flare kernel in *TRACE* WL. The *RHESSI* map was accumulated from 17:18:00 UT to 17:19:00 UT in the 50-100 keV energy range and the contour levels are 30%, 50%, 70%, and 90% of the maximum counts. The WL contours in (e, f) outline the δ spot region related to the flare. The FOV is $150'' \times 150''$.

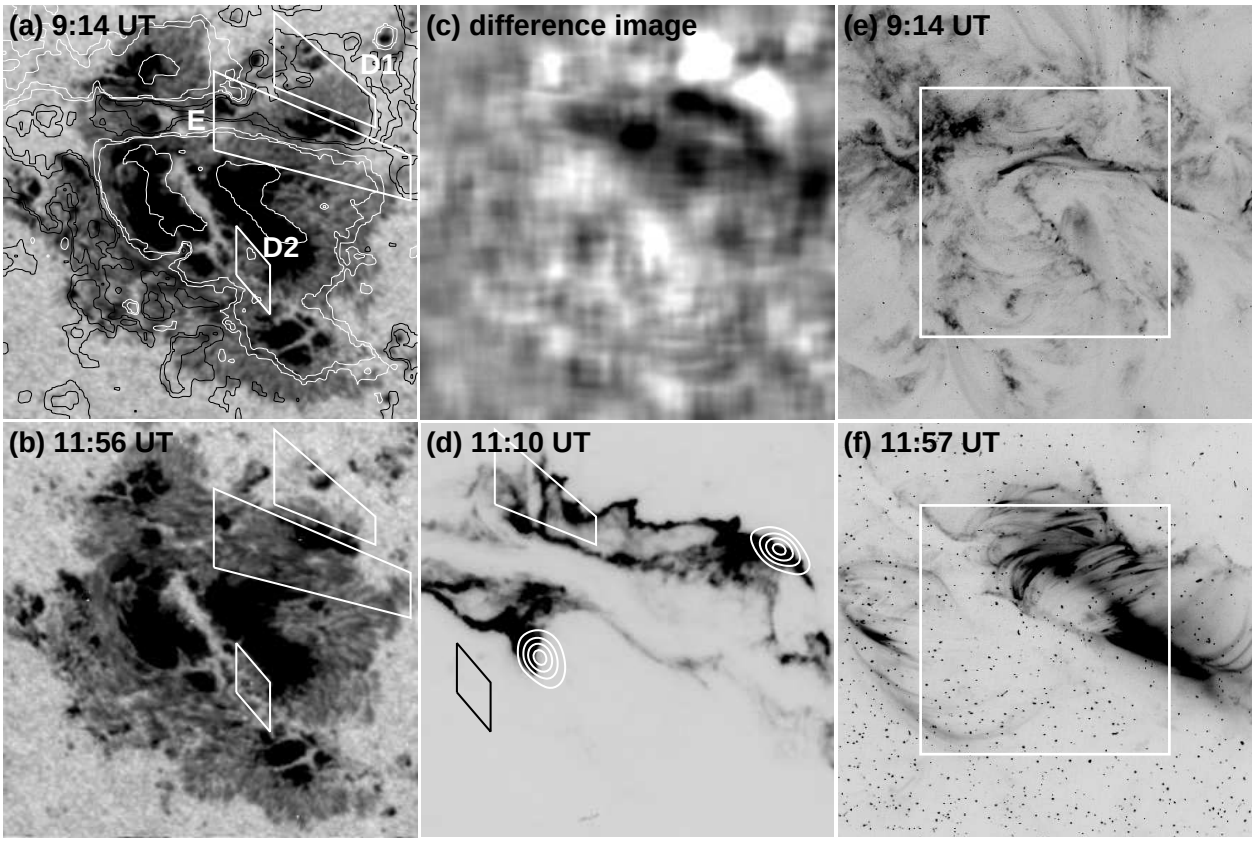

Fig. 6.— X17 flare on 2003 October 28. All panels show similar images as in Figure 1, except that (d) is a *TRACE* 1600 Å image with superimposed *RHESSI* 50-100 keV hard X-ray contours (levels are 30%, 50%, 70%, and 90% of the maximum counts) accumulated from 11:09:30 UT to 11:10:30 UT. The boxes in (e) and (f) represent the FOV in (a)-(d), which is $150'' \times 150''$. Note that the center of panel (d) has a $70''$ shift to the west in order to show the complete flare morphology.

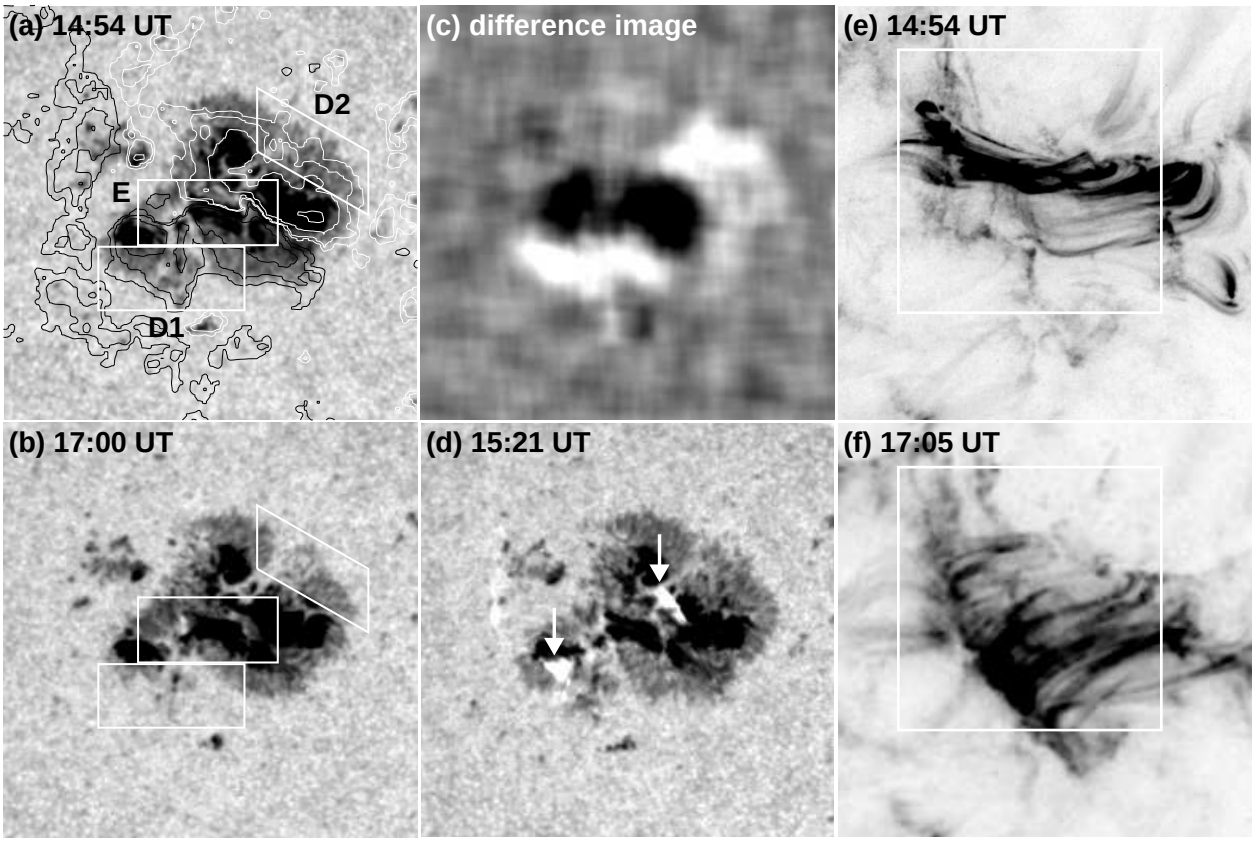

Fig. 7.— X2.3 flare on 2000 June 6. All panels show similar images as in Figure 1, except that (e) and (f) are *TRACE* 171 Å images. The magnetic contour levels in (a) are ± 150, 300, 700, and 1400 G. The boxes in (e) and (f) represent the FOV in (a)-(d), which is 130″ × 130″.

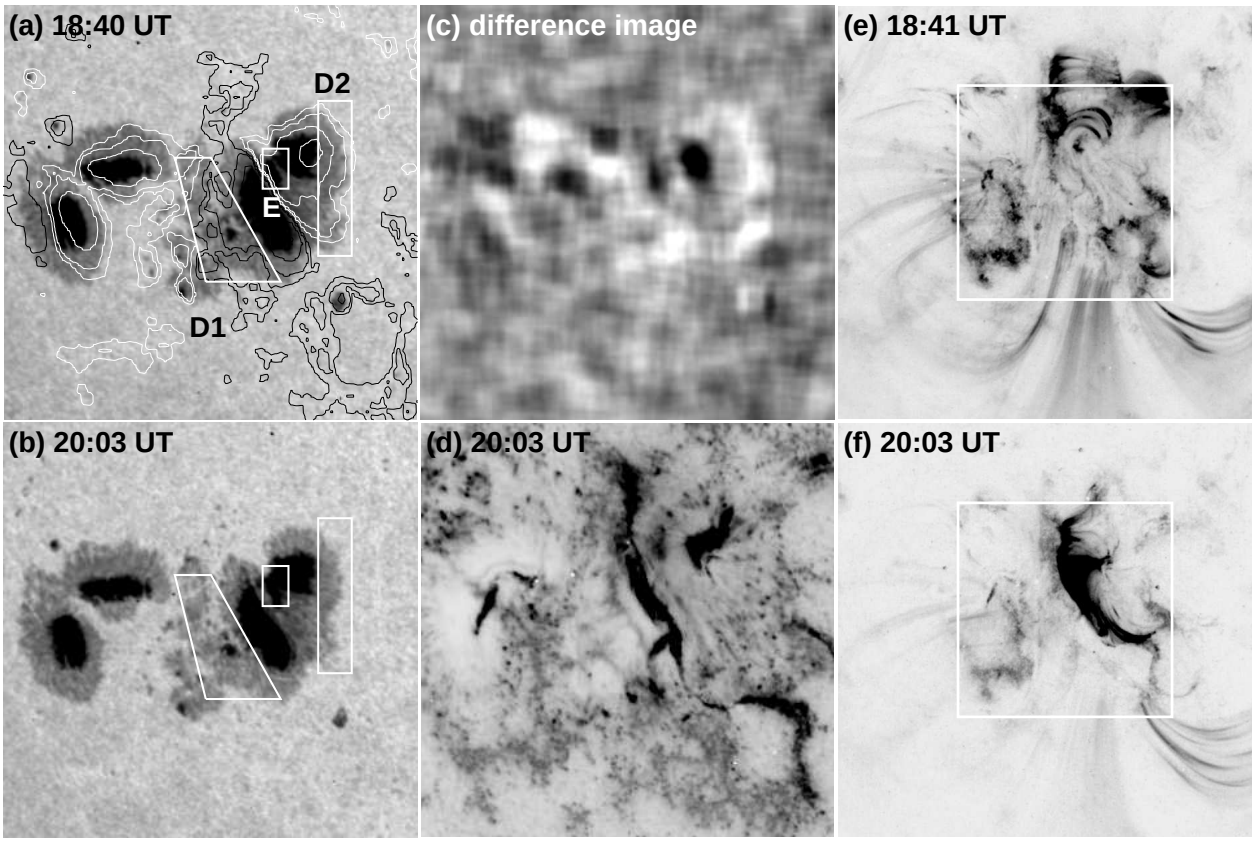

Fig. 8.— Same as Figure 7, but for the X5.6 flare on 2001 April 6. The boxes in (e) and (f) represent the FOV in (a)-(d), which is $160'' \times 160''$.

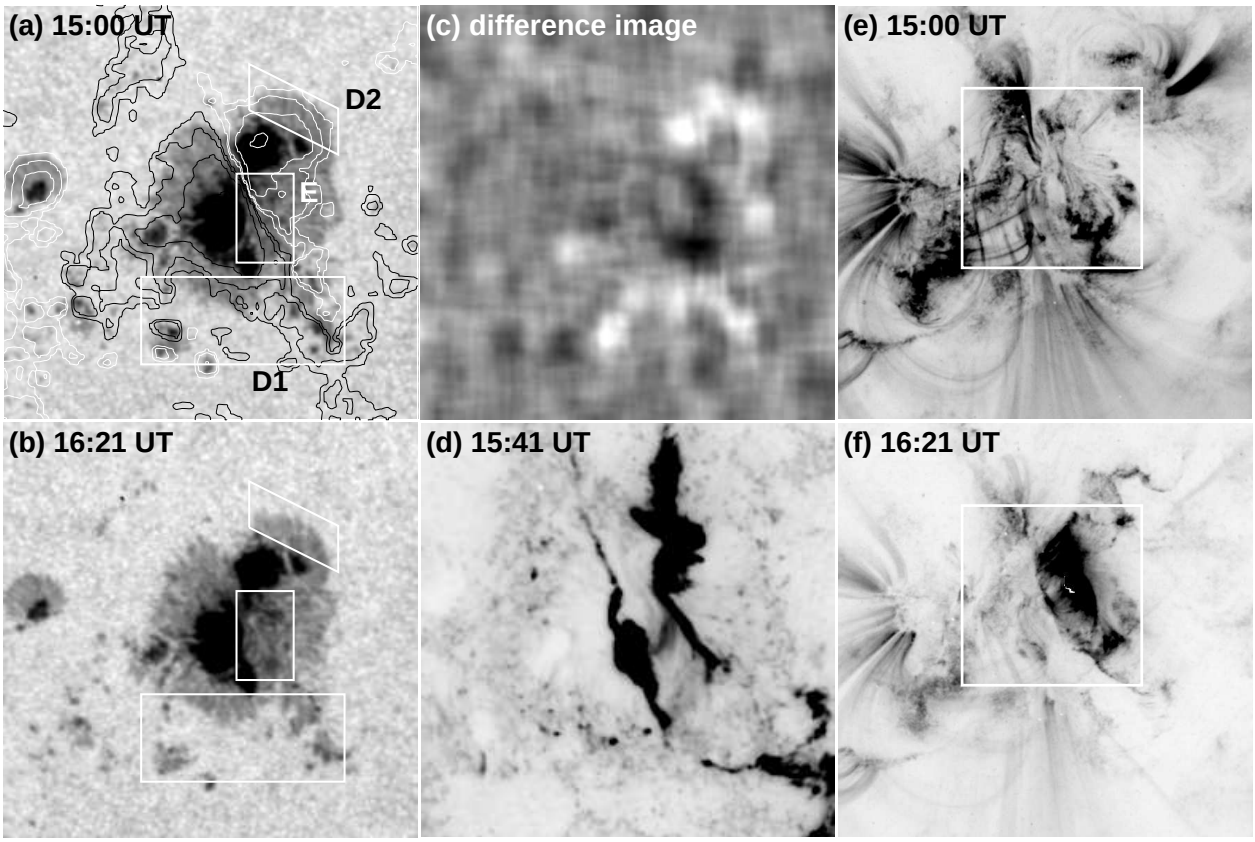

Fig. 9.— Same as Figure 7, but for the M7.9 flare on 2001 April 9. The boxes in (e) and (f) represent the FOV in (a)-(d), which is $130'' \times 130''$.

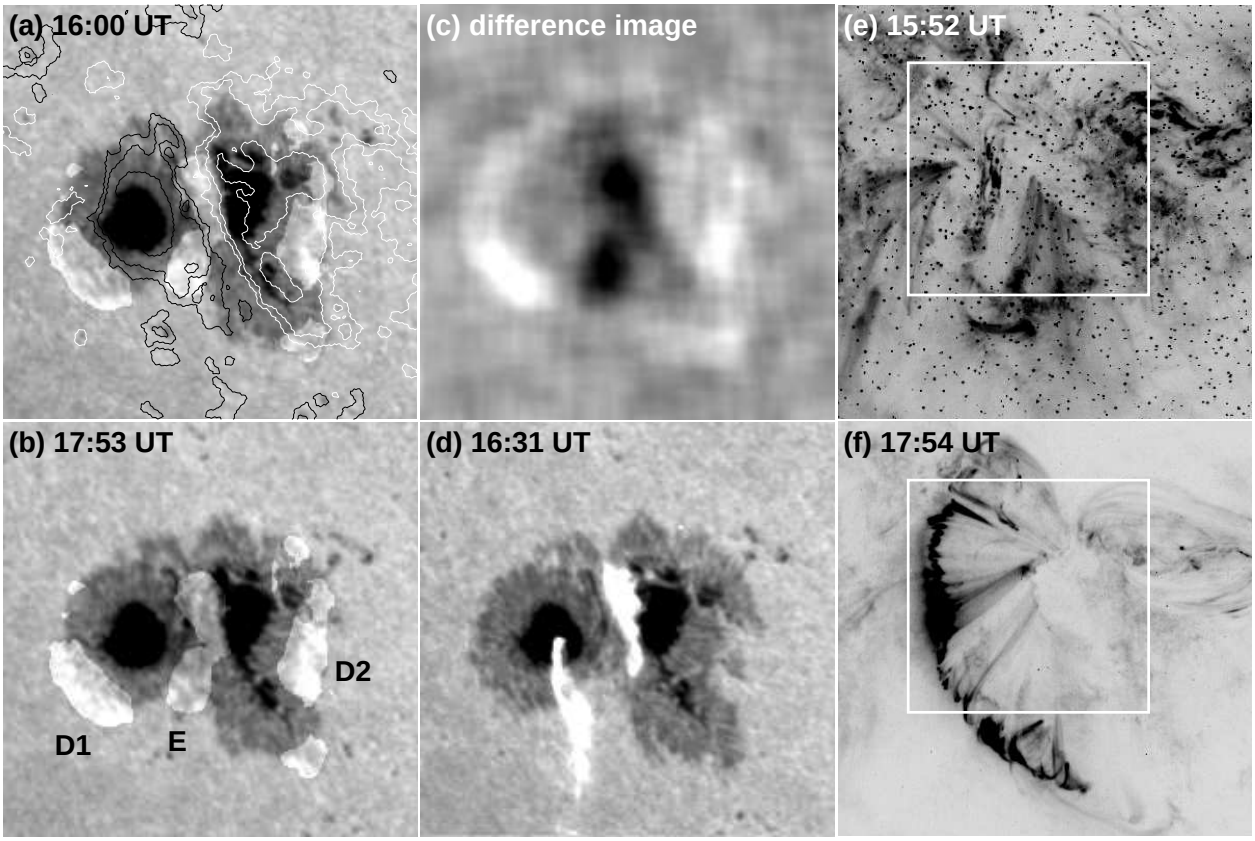

Fig. 10.— Same as Figure 7, but for the X5.3 flare on 2001 August 25. BBSO line-of-sight magnetogram contours at 16:13 UT are superimposed onto (a). High-lights in (a) and (b) are areas of decaying penumbra (D1 and D2) and darkening inner penumbra (E). The boxes in (e) and (f) represent the FOV in (a)-(d), which is $120'' \times 120''$.

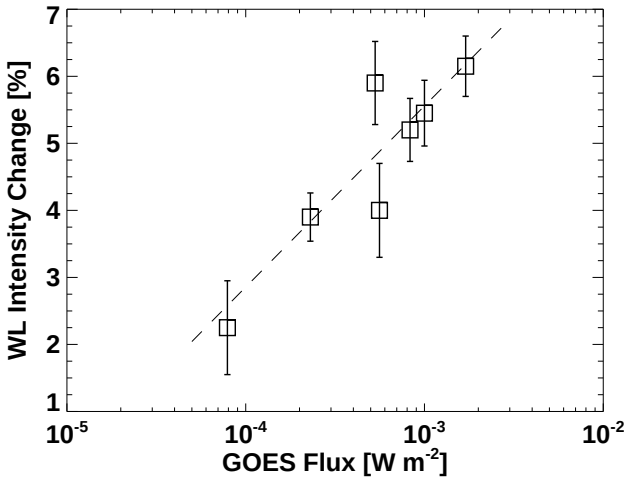

Fig. 11.— Scatter plot of the average intensity change of penumbral decay against *GOES* X-ray flux. The dashed line is a least-squares linear fit to all seven events with the correlation coefficient of 0.91. The error bars are standard deviation determined individually for each event by calculating the fluctuation in the time profile of mean intensity in a quiet Sun region.

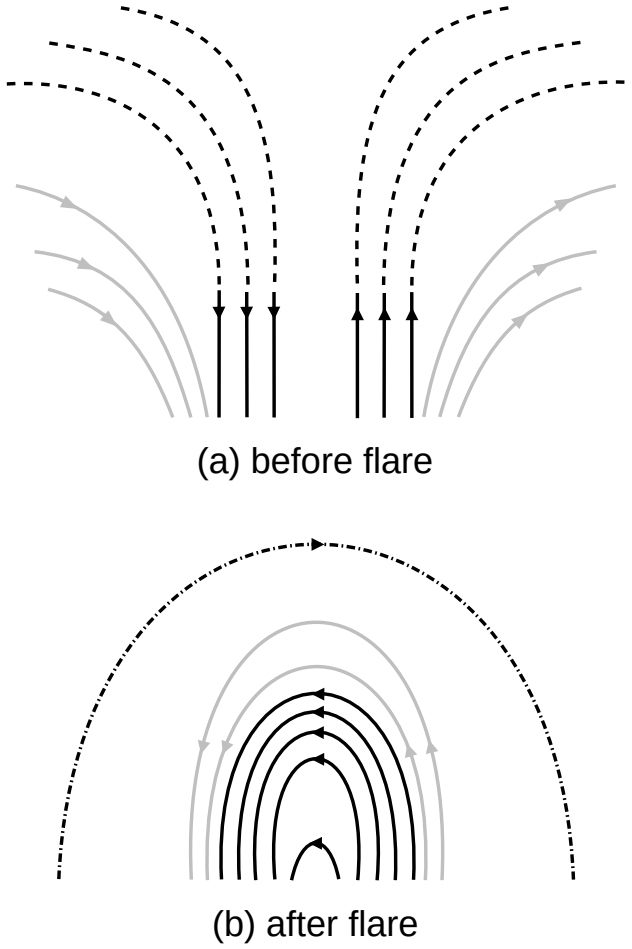

Fig. 12.— A schematic picture interpreting our observations. (a) Initial magnetic field configuration before the flare. Penumbral fields are in *grey* and umbral fields are in *black*. (b) Magnetic field configuration in the post-flare state. The dash-dot line represents the connection between two points far apart, which may form the large-scale arcade structure of CMEs.

REFERENCES

Antiochos, S. K., Devore, C. R., & Klimchuk, J. A. 1999, ApJ, 510, 485

Carmichael, H. 1964, in The Physics of Solar Flares, ed. W. N. Hess (NASA SP-50; Washington: NASA), 451

Chen, W., et al. 2005, in preparation

Deng, N., Liu, C., Yang, G., Wang, H., & Denker, C. 2003, ApJ, submitted

Domingo, V., Fleck, B., & Poland, A. I. 1995, Sol. Phys., 162, 1

Freeland, S. L., & Handy, B. N. 1998, Sol. Phys., 182, 497

Gaizauskas, V., Harvey, K. L., & Proulx, M. 1994, ApJ, 422, 883

Gaizauskas, V., Mandrini, C. H., Démoulin, P., Luoni, M. L., & Rovira, M. G. 1998, A&A, 332, 353

Hagenaar, H. J. 2001, ApJ, 555, 448

Hagyard, M. J., Smith, J. B. Jr., Teuber, D., & West, E. A. 1984, Sol. Phys., 91, 115

Handy, B. N., et al. 1999, Sol. Phys., 187, 229

Hirayama, T. 1974, Sol. Phys., 34, 323

Kopp, R. A., & Pneuman, G. W. 1976, Sol. Phys., 50, 85

Kosovichev, A. G., & Zharkova, V. V. 1999, Sol. Phys., 190, 459

Kosovichev, A. G., & Zharkova, V. V. 2001, ApJ, 550, L105

Krucker, S., Fivian, M. D., & Lin, R. P. 2005, Advances in Space Research, submitted

Kurokawa, H., Wang, T., & Ishii, T. T. 2002, ApJ, 572, 598

Künzel, H. 1960, Astron. Nachr., 285, 271

Li, W., et al. 1999, Magnetic Fields and Solar Processes, ed. A. Wilson, ESA SP Ser., 448, 169

Lin, R. P., et al. 2002, Sol. Phys., 210, 3

Liu, Y., & Zhang, H. 2001, A&A, 372, 1019

Liu, Y., & Zhang, H. 2002, A&A, 386, 646

Martínez Pillet, V., Lites, B. W., Skumanich, A. P., & Seagraves, P. 1994, Solar Active Region Evolution: Comparing Models with Observations, eds. Balasubramaniam, K. S. & Simon, G. W., ASP Conf. Ser., 68, 244

Metcalf, T. R., Alexander, D., Hudson, H. S., & Longcope, D. W. 2003, ApJ, 595, 483

Moore, R. L., Hurford, G. J., Jones, H. P., & Kane, S. R. 1984, ApJ, 276, 379

Parker, E. N. 1963, ApJS, 77, 8

Qiu, J., Lee, J., & Gary, D. E. 2004, ApJ, 603, 335

Sammis, I., Tang, F., & Zirin, H. 2000, ApJ, 540, 583

Scherrer, P. H., et al. 1995, Sol. Phys., 162, 129

Schmieder, B., et al. 1994, Sol. Phys., 150, 199

Schrijver, C. J., et al. 1999, Sol. Phys., 187, 261

Severny, A. B. 1964, ARA&A, 2, 363

Shi, Z., & Wang, J. 1994, Sol. Phys., 149, 105

Spirock, T. J., Yurchyshyn, V., & Wang, H. 2002, ApJ, 572, 1072

Sturrock, P. A. 1966, Nature, 221, 695

Sweet, P. A. 1958, Electromagnetic Phenomena in Cosmical Physics, ed. B. Lehnert (NY: Cambridge Univ. Press), IAU Symp. 6, 123

Tanaka, K. 1991, Sol. Phys., 136,133

Tang, F. 1983, Sol. Phys., 89, 43

Tang, F. & Wang, H. 1993, Sol. Phys., 143, 107

Wang, H. 1992, The Solar Cycle, ed. K. L. Harvey, ASP Conf. Ser., 27, 97

Wang, H., Ewell, M. W., Zirin, H., & Ai, G. 1994, ApJ, 424, 436

Wang, H., Ji, H., Schmahl, E. J., Qiu, J., Liu, C., & Deng, N. 2002a, ApJ, 580, L177

Wang, H., Liu, C., Deng, Y., Zhang, H. 2005, in preparation

Wang, H., Liu, C., Qiu, J., Deng, N., Goode, P. R., & Denker, C. 2004a, ApJ, 601, L195

Wang, H., Qiu, J., Jing, J., Spirock, T. J., Yurchyshyn, V., Abramenko, V., Ji, H., & Goode, P. R. 2004b, ApJ, 605, 931

Wang, H., Spirock, T. J., Qiu, J., Ji, H., Yurchyshyn, V., Moon, Y., Denker, C. & Goode, P. R. 2002b, ApJ, 576, 497

Wang, H., & Tang, F. 1993, ApJ, 407, L89

Yurchyshyn, V. 2003, AGU, FMSH, 22, 6

Yurchyshyn, V., Wang, H., Abramenko, V., Spirock, T. J., & Krucker, S. 2004, ApJ, 605, 546

Zirin, H. 1988, Astrophysics of the Sun (Cambridge Univ. Press)

Zirin, H., & Liggett, M. A. 1987, Sol. Phys., 113, 267

Zirin, H., & Tanaka, K. 1973, Sol. Phys., 32, 173

Zirin, H., & Wang, H. 1993, Sol. Phys., 144, 37

Zvereva, A. M., & Severny, A. B. 1970, Izv. Krymskoi Astrofiz. Obs., 41-42, 97